J. Fluid Mech. (2003), *vol.* 492, *pp.* 131–145.
DOI: 10.1017/S0022112003005585 Printed in the United Kingdom

Comparing the two-dimensional cascades of vorticity and a passive scalar

By THOMAS DUBOS AND ARMANDO BABIANO

IPSL/Laboratoire de Météorologie Dynamique, École Polytechnique 91128 Palaiseau Cedex, France

(Received 2 January 2003 and in revised form 30 April 2003)

We compare two-dimensional vorticity and passive scalar cascades seen as a gradient enhancement process. Our criteria are based on conditional averages of the first and second Lagrangian derivatives of vorticity and passive scalar gradients in relation to the local flow geometry. In order to interpret these criteria, transient properties are derived for random vorticity and scalar fields, showing that the second-order Lagrangian derivatives of vorticity and passive scalar gradients may behave differently. Cascades obtained in numerical simulations of decaying and forced incompressible turbulence are analysed. First-order analysis reveals that the direct cascade in elliptic domains is more efficient than previously suspected. While several first-order diagnostics collapse to a single curve for vorticity and passive scalars, second-order diagnostics consistently show that the vorticity gradient exhibits faster temporal fluctuations than the passive scalar gradient, a property which we anticipate qualitatively in the study of random fields.

1. Introduction

Two-dimensional vorticity is a Lagrangian-conserved scalar quantity in the absence of sources and sinks. It formally obeys the same advection equation as a passive tracer and the direct cascade of vorticity variance (enstrophy) is considered in theories as the process of stretching and folding of passive vorticity filaments, creating smaller and smaller scales in the vorticity field (Kraichnan 1971; Falkovich & Lebedev 1994). The effectiveness of this process crucially depends on how the filaments are aligned with respect to the external straining field (Saffman 1971). However, unlike the linear problem of passive advection, the dynamics of vorticity is nonlinear due to the direct connection between velocity and vorticity. This fundamental difference, and subsequently the effect of nonlinear processes on the alignment structure, should distinguish the enstrophy cascade from the transfer of passive scalar variance to small scales at some point (Babiano *et al.* 1987).

It is well known that the two-dimensional dynamics of a passive scalar is generically characterized by geometrical alignments of the scalar gradient with preferred directions prescribed by the flow (Okubo 1970; Weiss 1991; Protas, Babiano & Kevlahan 1999; Lapeyre, Klein & Hua 1999; Klein, Hua & Lapeyre 2000). It is therefore natural to try to distinguish active and passive scalars using their alignment properties in connection with a complex distribution of strain. In particular, a basic issue consists of understanding whether each kind of topological domain which manifest the non-homogeneous character of the flow may be associated with alignment properties that differ between vorticity and passive scalar (Lapeyre, Hua & Klein 2001). Diagnostics used in this work are global spatial averages based on a local

analysis that is eventually restricted to either elliptic or hyperbolic regions. While a transient difference is observed in the first states of vorticity and passive scalar cascades, the diagnostics used in (Lapeyre *et al.* 2001) collapse to a single value in the long term and it is not possible to characterize their difference. We suggest that more local quantities should be more able to reveal the expected difference.

The main purpose of the present contribution is to revisit this problem and propose suitable indicators for more detailed statistics in physical space. An element of the problem is that the spatial structure of vorticity and passive scalar fields in physical space is qualitatively very similar and it is impossible to decide whether the local differences are to be attributed to a random fluctuation or a dynamical origin. On the other hand, geometrical properties are much more explicit in physical space than in Fourier space in which they result only in phase relations that are not simple to capture. We will therefore restrict our analysis to the physical space using, as in Lapeyre *et al.* (2001), objective criteria that significantly enhance the Okubo–Weiss criterion which classifies spatial regions as elliptic or hyperbolic (Klein *et al.* 2000). The point is that the evolution of the scalar gradient under the action of a given flow is invariant under a change of rotating reference frame. Hence, in order to retain a certain amount of locality while ensuring that the random fluctuations are smoothed out by an averaging operation, we will use as diagnostics a conditional average involving local, frame-invariant characteristics of the flow. We can state two main results of our analysis. First, it appears that the transfer of vorticity and passive scalar variance in elliptic regions is more efficient than previously suspected. Second, we extend our study to a second-order statistic and show that only these are successful in revealing the active-passive difference.

The organization of the paper is as follows. In § 2 we sketch the main results obtained from the Lagrangian analysis of the gradients growth. They are used in § 3 to define quantities that diagnose the cascades following the guidelines found above. In § 4 we present several numerical experiments on two-dimensional turbulence with vorticity and passive scalars. We diagnose them and discuss the observations. Finally, the work is summarized and its implications are discussed.

2. Lagrangian dynamics of scalar gradients

2.1. *Stretching and rotation*

We outline in this section the basic ingredients of the two-dimensional Lagrangian dynamics of scalar gradients. Considering a scalar T transported by an incompressible fluid. Neglecting the molecular diffusivity, the evolution equations for T and its gradient $\boldsymbol{q} = \nabla T$ are:

$$\frac{\partial T}{\partial t} + \boldsymbol{u} \cdot \nabla T = 0, \tag{2.1}$$

$$\frac{\mathrm{d}}{\mathrm{d}t}\boldsymbol{q} + \boldsymbol{A}^T \boldsymbol{q} = 0, \tag{2.2}$$

where $\boldsymbol{A}^T$ denotes the transpose matrix of the velocity gradient $A_{ij} = \partial_j u_i$ and $\mathrm{d}/\mathrm{d}t$ is the Lagrangian derivative. The velocity gradient $\boldsymbol{A} = \boldsymbol{S} + \frac{1}{2}\omega \boldsymbol{J}$ decomposes into the symmetric strain-rate tensor

$$\boldsymbol{S} = \tfrac{1}{2}(\boldsymbol{A} + \boldsymbol{A}^T) \sim \tfrac{1}{2}\begin{bmatrix} \sigma & \\ & -\sigma \end{bmatrix}$$

that stretches $\boldsymbol{q}$ and the vorticity ω that rotates it. Here $4\sigma^2 = -\det \boldsymbol{S}$ and $\boldsymbol{J}$ refers the two-dimensional antisymmetric unit matrix.

The question one asks is whether the growth and orientation of the scalar gradient can be predicted from the local properties of the velocity field such as the velocity gradient $\boldsymbol{A}$. The difficulty comes from the time dependence of $\boldsymbol{S}$ since $\boldsymbol{S}$, in contrast to ω, evolves along a Lagrangian path even in the absence of sources and sinks. Under the assumption of slow evolution $\mathrm{d}S/\mathrm{d}t \ll \sigma^2$, (2.2) reduces to a simple eigenvalue problem (Okubo 1970; Weiss 1991). The evolution of $\boldsymbol{q}$ depends on whether $-\boldsymbol{A}^T$ has real or imaginary eigenvalues, which can be deduced from the sign of

$$Q = -4 \det \boldsymbol{A} = \sigma^2 - \omega^2. \tag{2.3}$$

If the so-called Okubo–Weiss criterion Q, diagnosing the competition between stretching and rotation, is positive then $-\boldsymbol{A}^T$ has two real and opposite eigenvalues and the gradient is predicted to grow exponentially and to align with the corresponding eigenvector. Conversely, if $Q < 0$, the eigenvalues are purely imaginary and the gradient is expected to rotate without growing. Regions where gradients grow are called hyperbolic while no-growth regions are called elliptic. Particle dispersion, alignment properties and other features of two-dimensional dynamics have been discussed by categorizing the incompressible turbulent field according to (2.3) (Ohkitani 1991; Elhmaidi, Provenzale & Babiano 1993; Provenzale 1999; Protas *et al.* 1999; Babiano 2001). The consistency of such a categorization is based on the diagnostic relation $Q = -2\Delta P$ between Q and the Laplacian of pressure (Larchevêque 1993).

2.2. *Objective parameters*

The assumption of slow strain-rate evolution is known to fail in many situations, but not for instance at saddle points and in vortex cores (Basdevant & Philipovitch 1994). Instead of purely neglecting the temporal evolution of $\boldsymbol{S}$, one can partly take it into account by decomposing it into the fluctuation $\mathrm{d}\sigma/\mathrm{d}t$ of its eigenvalues σ and $-\sigma$ and the rotation of its eigenvectors at the angular speed $\mathrm{d}\phi/\mathrm{d}t$:

$$\frac{\mathrm{d}\boldsymbol{S}}{\mathrm{d}t} = \frac{1}{\sigma}\frac{\mathrm{d}\sigma}{\mathrm{d}t}\boldsymbol{S} - 2\frac{\mathrm{d}\phi}{\mathrm{d}t}\boldsymbol{J}\boldsymbol{S}. \tag{2.4}$$

The rotation of the strain-rate axes is taken into account by expressing (2.2) on the strain basis (Dresselhaus & Tabor 1991). The role of vorticity is played by an effective rotation $\omega + 2\mathrm{d}\phi/\mathrm{d}t$ and the competition between stretching and rotation is measured by the non-dimensional parameter introduced in Lapeyre *et al.* (1999):

$$r \equiv \frac{\omega + 2\mathrm{d}\phi/\mathrm{d}t}{\sigma}. \tag{2.5}$$

In hyperbolic regions ($|r| < 1$), exponential growth is predicted together with an alignment of the scalar gradient with an eigenvector of $S - (\omega + 2\mathrm{d}\phi/\mathrm{d}t)\,J$. This prediction is supported by numerical experiments (Lapeyre *et al.* 1999). In elliptic regions ($|r| > 1$), the no-growth prediction can be improved by also taking into account $\mathrm{d}\sigma/\mathrm{d}t$ through the non-dimensional quantity (Klein *et al.* 2000):

$$s \equiv \frac{1}{\sigma^2}\frac{\mathrm{d}\sigma}{\mathrm{d}t}. \tag{2.6}$$

Let us stress here that the Okubo–Weiss criterion Q (equation (2.3)) is not invariant under a change of rotating reference frame. This could be *cured* by subtracting from the vorticity its global average. This would however be at the price of the locality, since the average vorticity is not accessible from a local point of view. It is a merit of the parameters r and s that they are frame indifferent and defined from only

local characteristics of the flow. In what follows, we shall therefore employ only such *objective* quantities when constructing our diagnostics.

3. Gradient evolution as a basis for local diagnostics

3.1. *Physical interpretation of Lagrangian derivatives*

The first-order Lagrangian derivative is both a local indicator of the cascade, as it measures the creation of small scales in the scalar field, and a geometric quantity through its connection to the strain-rate tensor $\boldsymbol{S}$:

$$\frac{\mathrm{d}}{\mathrm{d}t}q^2 = -2\boldsymbol{q}\cdot\boldsymbol{S}\cdot\boldsymbol{q}. \tag{3.1}$$

The sign of the production of scalar gradients by stirring depends on the orientation of $\boldsymbol{q}$ with respect to the compressional axis of the strain-rate tensor $\boldsymbol{S}$. If the angle is less than 45°, there will be production of gradient, and vice versa (Protas *et al.* 1999; Lapeyre *et al.* 2001; Dubos & Babiano 2002). The interpretation of (3.1) in terms of a cascade is therefore simple: a growth of the gradients indicates a direct cascade, and vice versa.

The second-order Lagrangian derivative, although slightly more difficult to interpret geometrically, provides complementary information on the growth process:

$$\frac{\mathrm{d}^2}{\mathrm{d}t^2}q^2 = \boldsymbol{q}\cdot\boldsymbol{N}\cdot\boldsymbol{q}, \tag{3.2}$$

$$\boldsymbol{N} = \sigma^2\delta_{ij} - 2\hat{\boldsymbol{S}}, \tag{3.3}$$

$$\hat{\boldsymbol{S}} = \frac{\mathrm{d}\boldsymbol{S}}{\mathrm{d}t} - \omega\boldsymbol{J}\boldsymbol{S}, \tag{3.4}$$

where the tensor $\boldsymbol{N}$ involves the corotational derivative of $\boldsymbol{S}$, $\hat{\boldsymbol{S}}$. The second-order Lagrangian derivative (3.2) gives information about the concavity or convexity of the curve $q^2(t)$. Thus in a hyperbolic region with potentially exponential growth, it can be expected to be positive. Conversely, a negative value would correspond to a temporal oscillation and an elliptic region.

The basic idea consisting of considering a local cascade-related quantity such as the growth rate of the scalar gradient and directly comparing the two fields corresponding to vorticity and passive scalar is however intractable. As an illustration we display in figure 1 the second Lagrangian time derivative of the squared gradient of vorticity (*a*) and passive scalar (*b*) in a stationary, large-scale forced simulation at resolution 1024^2 described in detail in Dubos & Babiano (2002). We focus on a 300×400 region containing a pair of vortices. Both fields $\mathrm{d}^2q_\omega^2/\mathrm{d}t^2$ and $\mathrm{d}^2q_T^2/\mathrm{d}t^2$ have an extremely similar spatial structure with tiny local discrepancies which cannot be straightforwardly attributed to a dynamical or random origin. In order to keep a certain amount of locality while ensuring that the random fluctuations are smoothed, for our diagnostics we will consider conditional averages of the first- and second-order Lagrangian derivatives of the scalar-gradient-squared norm.

3.2. *A kinematic property of vorticity*

The usefulness of the second-order Lagrangian derivative is most evident at the initial stage of a mixing process, before the advection has built a correlation between the scalar gradient and velocity fields. At this instant the scalar field is statistically independent of the velocity. Furthermore the spatial average $\langle \mathrm{d}q^2/\mathrm{d}t \rangle$ vanishes for both the vorticity gradient $\boldsymbol{q}_\omega$ and the passive scalar gradient $\boldsymbol{q}_T$. This first-order diagnostic thus contains no useful information on the average growth of the gradients.

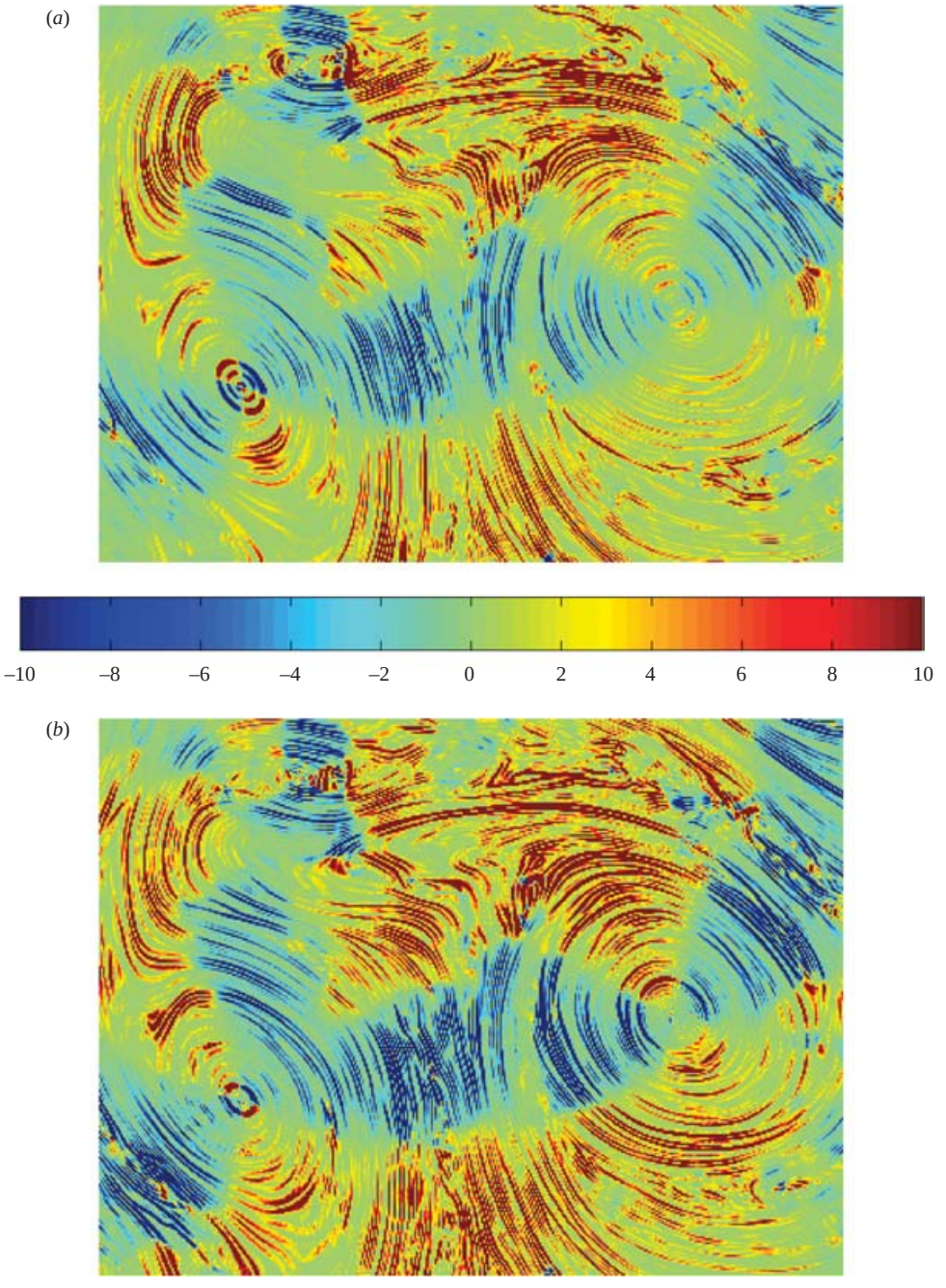

FIGURE 1. Second Lagrangian time derivative of the squared gradient of vorticity $\mathrm{d}q_\omega^2/\mathrm{d}t^2$ (*a*) and passive scalar $\mathrm{d}q_T^2/\mathrm{d}t^2$ (*b*) in a stationary, large-scale forced simulation. The unit is the spatial average of each field. Enlargement of a 300×400 area out of a 1024^2 box.

The missing information is provided by the second-order derivative because for short enough times

$$\langle q^2(t)\rangle \approx \langle q^2\rangle_{t=0} + t\left\langle \frac{\mathrm{d}}{\mathrm{d}t}q^2\right\rangle_{t=0} + \frac{t^2}{2}\left\langle \frac{\mathrm{d}^2}{\mathrm{d}t^2}q^2\right\rangle_{t=0}. \tag{3.5}$$

Given a tensor $\boldsymbol{M}$ and a random vector $\boldsymbol{q}$ independent of $\boldsymbol{M}$ with an isotropic distribution, a general result is

$$\langle \boldsymbol{q}\cdot\boldsymbol{M}\cdot\boldsymbol{q}\rangle = \tfrac{1}{2}\langle q^2\rangle \mathrm{Tr}\boldsymbol{M}. \tag{3.6}$$

Taking for $\boldsymbol{M}$ the tensor $\boldsymbol{N}$ (equation (3.3)) and using $\langle\sigma^2\rangle = \langle\omega^2\rangle = 2Z$ with Z the enstrophy of the flow gives for the passive scalar

$$\left\langle \frac{\mathrm{d}^2}{\mathrm{d}t^2} q_T^2 \right\rangle_{t=0} = 2Z \left\langle q_T^2 \right\rangle_{t=0} \tag{3.7}$$

so that passive scalar gradients always initially grow with a time scale given by the enstrophy Z. This is not true in general for vorticity. Indeed, assuming an initial energy spectrum peaked around a wavenumber k_0 (as in the simulation LARGE diagnosed in Lapeyre *et al.* (2001) and in what follows), the flow is quasi-stationary at short times because $\omega = -\Delta\psi \approx k_0^2\psi$, so that $\partial\omega/\partial t \approx 0$ and $\langle \mathrm{d}^2 q_\omega^2/\mathrm{d}t^2\rangle \approx 0$. There is therefore in this case on average an initial *stagnation* of the palinstrophy $\frac{1}{2}\langle q_\omega^2\rangle$.

From a more local point of view, one can use equation (3.6) to derive the following relation between conditional averages with respect to the strain-rate σ:

$$\frac{E\left(\mathrm{d}^2 q_T^2/\mathrm{d}t^2;\,\sigma\right)}{E\left(q_T^2;\,\sigma\right)} = \sigma^2. \tag{3.8}$$

This holds for the passive scalar gradient $\boldsymbol{q}_T$ which is initially independent of the velocity field but *not* for the vorticity gradient $\boldsymbol{q}_\omega$ which is correlated with the tensor $\hat{\boldsymbol{S}}$. Using (3.3) we find

$$\frac{E\left(\mathrm{d}^2 q_\omega^2/\mathrm{d}t^2;\,\sigma\right)}{E\left(q_\omega^2;\,\sigma\right)} = \sigma^2 - 2\frac{E(\boldsymbol{q}_\omega\cdot\hat{\boldsymbol{S}}\cdot\boldsymbol{q}_\omega;\,\sigma)}{E\left(q_\omega^2;\,\sigma\right)}. \tag{3.9}$$

Conditional averages should thus enable one to distinguish between regions where the vorticity gradients grow or decay, while passive scalar gradients initially grow everywhere in a statistical sense.

We exhibit here a special property of vorticity: its connection to the flow, which translates into correlations between the vorticity gradient $\boldsymbol{q}_\omega$ and the tensor $\hat{\boldsymbol{S}}$, modifies its cascade properties with respect to those of a passive scalar uncorrelated with the flow. We call this property 'kinematic' because it holds for a random field and does not require the flow to be turbulent, indicating that it only relies on the connection between the vorticity field and the flow and not on the statistical structure of a turbulent flow.† It is now to be determined whether this difference persists a long time after the passive scalar is put in a turbulent flow.

3.3. *Conditional diagnostics*

We have shown that the difference between vorticity and passive scalar detected by the second-order Lagrangian derivative of gradients is much larger when the spectrum is peaked. This spectrum corresponds to a linear relation between vorticity ω and stream function ψ:

$$\omega = k_0^2\psi. \tag{3.10}$$

In a turbulent field, this relation does not hold globally. However, it may hold locally in a coherent structure: relation (3.10) is a widely used empirical characterization of

† What we observe in what follows is that turbulence actually tends to bring the passive scalar and vorticity to a similar statistical structure and to hide this kinematic difference.

	First order $\frac{\mathrm{d}}{\mathrm{d}t}q^2 = -\boldsymbol{q}\cdot\boldsymbol{S}\cdot\boldsymbol{q}$	Second order $\frac{\mathrm{d}^2}{\mathrm{d}t^2}q^2 = \boldsymbol{q}\cdot\boldsymbol{N}\cdot\boldsymbol{q}$
Global	$h \equiv \dfrac{\langle \mathrm{d}q^2/\mathrm{d}t\rangle}{\langle q^2\rangle}$	$z \equiv \dfrac{\langle \mathrm{d}^2q^2/\mathrm{d}t^2\rangle}{\langle q^2\rangle}$
$r \equiv \dfrac{\omega + 2\mathrm{d}\phi/\mathrm{d}t}{\sigma}$	$h(r) \equiv \dfrac{E(\mathrm{d}q^2/\mathrm{d}t\,;\, r)}{E(q^2\,;\, r)}$	$z(r) \equiv \dfrac{E(\mathrm{d}^2q^2/\mathrm{d}t^2\,;\, r)}{E(q^2\,;\, r)}$
$s \equiv \dfrac{1}{\sigma^2}\dfrac{\mathrm{d}\sigma}{\mathrm{d}t}$	$h(s) \equiv \dfrac{E(\mathrm{d}q^2/\mathrm{d}t\,;\, s)_{\lvert r\rvert>1}}{E(q^2\,;\, s)_{\lvert r\rvert>1}}$	$z(s) \equiv \dfrac{E\left(\mathrm{d}^2q^2/\mathrm{d}t^2\,;\, s\right)_{\lvert r\rvert>1}}{E\left(q^2\,;\, s\right)_{\lvert r\rvert>1}}$

TABLE 1. Diagnostic quantities.

coherent structures (Lamb 1932; Batchelor 1967). One can approximately† identify them with the elliptic domains defined by the parameter r (equation (2.5)). A first set of diagnostics will thus be obtained by conditional averages with respect to r.

In elliptic domains, the second parameter s (equation (2.6)) is important for the gradient dynamics (Klein *et al.* 2000). This leads us to also consider conditional averages with respect to s and limited to elliptic domains ($|r| > 1$). Our diagnostics will therefore be the four quantities $h(r)$, $h(s)$, $z(r)$ and $z(s)$ summarized in table 1. They all provide a time scale for the cascade, h (first-order diagnostic) being the inverse of a time and z (second-order diagnostic) the inverse of a squared time.

4. Numerical experiments and results

4.1. *Numerical experiments*

The diagnostics defined in the previous section are computed on vorticity and passive scalar fields obtained from direct numerical simulations of incompressible two-dimensional turbulence. The Navier–Stokes equations are solved using a fully dealiased pseudo-spectral code at resolution 1024^2. One or two passive scalars are present in the flow and obey the same equation as vorticity. We consider three different experiments, all using a Newtonian viscosity/diffusivity:

(i) The simulation labelled 'SMALL' in Lapeyre *et al.* (2001), kindly provided by Guillaume Lapeyre. This is a simulation of decaying turbulence containing one passive scalar:

$$\frac{\partial\omega}{\partial t} + \nabla\cdot(\omega\boldsymbol{u}) = \nu\Delta\omega, \tag{4.1}$$

$$\frac{\partial T}{\partial t} + \nabla\cdot(T\boldsymbol{u}) = \nu\Delta T. \tag{4.2}$$

Vorticity and passive scalar are initialized with a prescribed spectrum and random, uncorrelated phases. The chosen spectrum is wide, $Z(k) = Z_T(k) \propto k^{-1}$. We will

† It is clear that the condition $|r| < 1$ does not uniquely identify coherent structures (Basdevant & Philipovitch 1994). There are for instance points in the turbulent background surrounding the vortices that satisfy $|r| < 1$. Nevertheless the cores of coherent vortices all satisfy $|r| < 1$.

consider the initial random fields and the state reached after about 100 turnover times. At that instant, both cascades present the same characteristics according to Lapeyre *et al.*'s analysis. The flow is dominated by two large-scale vortices but the enstrophy and passive scalar spectra remain close to a k^{-1} law at small scales, indicating still active cascades.

(ii) A simulation equivalent to that labelled 'LARGE' in Lapeyre *et al.* (2001). This is again decaying turbulence but with a different initial spectrum, concentrated at a single wavenumber $k_0 = 10$. The difference is now that two passive scalars with independent initial conditions are inserted. We will consider the initial state and the final state obtained after 70 turnover times. The flow then contains many vortices and filaments, though the development of turbulence is not as advanced as in SMALL.

(iii) A forced, statistically stationary simulation, containing two passive scalars. The forcing consists of keeping constant the amplitude of the wavenumber $k = 4$. Due to the inverse energy cascade, a large-scale dissipation is necessary to enforce the stationarity of the vorticity field. For the sake of the comparison, this unphysical dissipation is also employed for the passive scalars. The equations governing the vorticity and the two passive scalars are thus

$$\frac{\partial \omega}{\partial t} + \nabla \cdot (\omega \boldsymbol{u}) = \gamma \Delta^{-1} \omega + \nu \Delta \omega + f_\omega, \tag{4.3}$$

$$\frac{\partial T}{\partial t} + \nabla \cdot (T \boldsymbol{u}) = \gamma \Delta^{-1} T + \nu \Delta T + f_T. \tag{4.4}$$

Although long-time, asymptotic properties are best observed in statistically stationary turbulence, decaying simulations avoid the problem of defining the forcing method and the large-scale dissipation. The presence of two passive scalars ensures that an eventually observed vorticity–scalar difference is indeed significant. The two scalars might present slightly different values of a given diagnostic and only vorticity–scalar differences above this scalar–scalar fluctuation can be considered to be due to the dynamical character of vorticity.

At the final instant of all these simulations, the diagnostics h and z (table 1) based on global spatial averages take identical values for vorticity and a passive scalar.

4.2. *Results*

4.2.1. *Kinematic properties*

We checked relation (3.8) and the discrepancy between vorticity and passive scalar for two pairs of random fields, each pair consisting of a vorticity and a passive scalar field with the same prescribed spectrum. The first pair has a peaked spectrum and the second a broad spectrum $Z(k) = Z_T(k) \propto k^{-1}$. We present in figure 2 the ratios $z_T(\sigma)$ and $z_\omega(\sigma)$ obtained in each case:

$$z_T(\sigma) \equiv \frac{E\left(\mathrm{d}^2 q_T^2/\mathrm{d}t^2; \sigma\right)}{E\left(q_T^2; \sigma\right)}, \tag{4.5}$$

$$z_\omega(\sigma) \equiv \frac{E\left(\mathrm{d}^2 q_\omega^2/\mathrm{d}t^2; \sigma\right)}{E\left(q_\omega^2; \sigma\right)}. \tag{4.6}$$

First, we do indeed have $z_T(\sigma) = \sigma^2$ as expected from equation (3.8). It turns out that $z_\omega(\sigma)$ is an affine function of σ^2 with slope one and $z_T(\sigma) - z_\omega(\sigma)$ is a positive constant z_0. According to relation (3.9), this means that the correlation $E(\boldsymbol{q}_\omega \cdot \hat{\boldsymbol{S}} \cdot \boldsymbol{q}_\omega; \sigma)$ is proportional to $E\left(q_\omega^2; \sigma\right)$. This is an empirical observation which seems very difficult to derive *ab initio*. It is nevertheless possible to obtain the

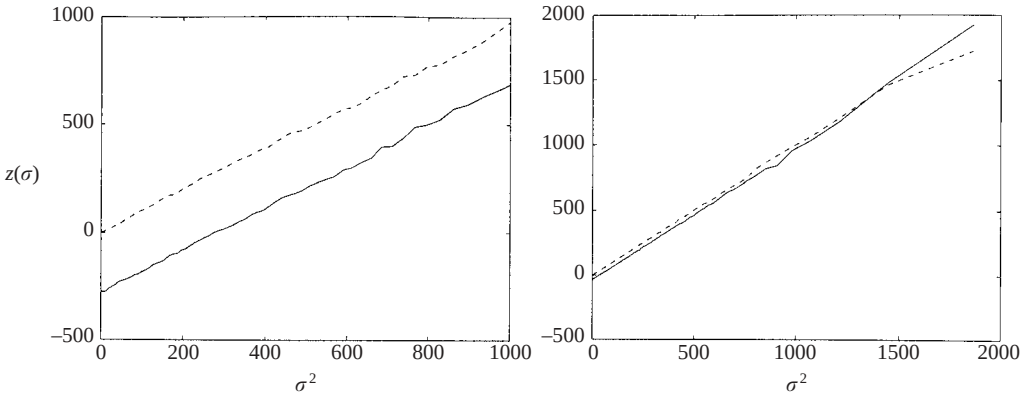

FIGURE 2. Diagnostics $z_\omega(\sigma)$ (solid) and $z_T(\sigma)$ (dashed) for random fields of passive scalar T and vorticity ω with the same spectrum. (*a*) Spectrum peaked around wavenumber $k = 10$. (*b*) Broad spectrum $Z(k) = Z_T(k) \propto k^{-1}$.

value of the constant z_0 in experiment LARGE by taking into account the fact that $E(q_\omega^2; \sigma)$ is actually independent of σ (and therefore equal to $\langle q_\omega^2 \rangle$), which we checked numerically in our data. Indeed if we let $p(\sigma)$ be the probability density function of σ we have

$$\begin{aligned}\left\langle \frac{\mathrm{d}^2}{\mathrm{d}t^2} q_\omega^2 \right\rangle &= \int_0^\infty E\left(\frac{\mathrm{d}^2}{\mathrm{d}t^2} q_\omega^2; \sigma\right) p(\sigma)\,\mathrm{d}\sigma \\ &= \int_0^\infty E\left(q_\omega^2; \sigma\right) z_\omega(\sigma) p(\sigma)\,\mathrm{d}\sigma \\ &= \left\langle q_\omega^2 \right\rangle \int_0^\infty (\sigma^2 - z_0) p(\sigma)\,\mathrm{d}\sigma \\ &= \left\langle q_\omega^2 \right\rangle (\langle \sigma^2 \rangle - z_0).\end{aligned}$$

Since in experiment LARGE $\langle \mathrm{d}^2 q_\omega^2 / \mathrm{d}t^2 \rangle = 0$, we find $z_0 = \langle \sigma^2 \rangle = 2Z$. In the present case, $2Z = 280$ which agrees rather well with figure 2(*a*). The inequality $z_T(\sigma) > z_\omega(\sigma)$ fits with the fact that the vorticity cascade (solid) is initially less efficient than the passive scalar cascade (dashed) (Holloway & Kristmannsson 1984; Lapeyre *et al.* 2001). It is worth noting that below a certain value of the strain rate σ, $z_\omega(\sigma)$ takes negative values. This is required by the global stagnation of palinstrophy and means that in regions of low strain the vorticity gradients will initially decay. Such a decay is impossible for a passive scalar.

However this effect strongly depends on the spectra as is shown by figure 2(*b*): in the case of a broad spectrum, the quantities $z_T(\sigma)$ and $z_\omega(\sigma)$ collapse to a single curve. Furthermore, as time passes the passive scalar field acquires a correlation with the velocity field which breaks relation (3.8) and the curves $z_T(\sigma)$ and $z_\omega(\sigma)$ are attracted towards each other. We illustrate this in figure 3, displaying the curves $z_\omega(\sigma)$ (solid) and $z_T(\sigma)$ (dashed) at later times: after 10 turnover times (crosses) and after 70 turnover times (circles). The affine dependence of $z(\sigma)$ on σ is lost, and the two curves approach each other and collapse in the long term. Also we found in the final stages of experiments SMALL and FORCED that $z_T(\sigma)$ and $z_\omega(\sigma)$ are also identical, leading us to study the other four diagnostics $h(r)$, $h(s)$, $z(r)$, $z(s)$.

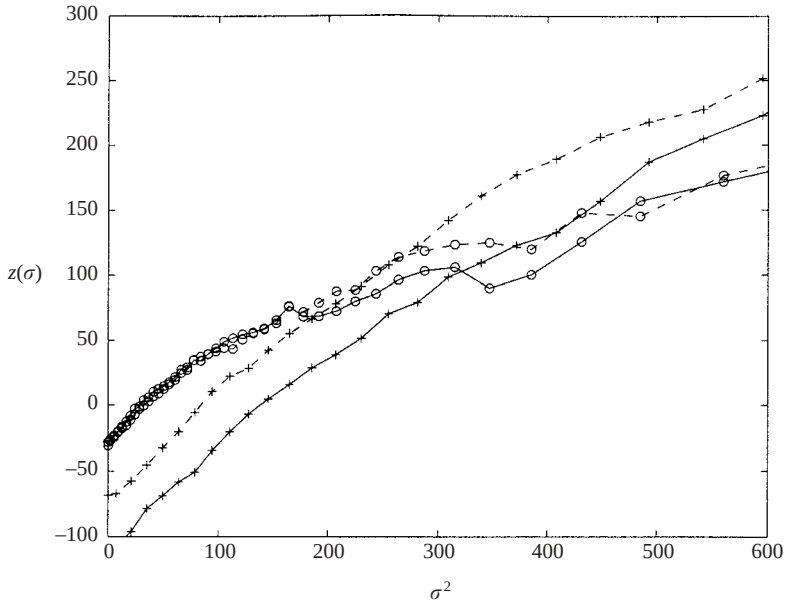

FIGURE 3. Diagnostics $z_\omega(\sigma)$ (solid) and $z_T(\sigma)$ (dashed) for passive scalar T and vorticity ω in experiment LARGE after 10 turnover times (crosses) and after 70 turnover times (circles).

4.2.2. *First-order diagnostics: local cascade efficiency*

We present in figure 4 the diagnostics based on the first Lagrangian derivative, $h(r)$ (figure 4*a*) and $h(s)$ (figure 4*b*). Experiments LARGE, SMALL and FORCED are presented from top to bottom.

The r-conditioned growth rate $h(r)$ is positive and increases when $|r|$ decreases ($\alpha \equiv (1+r^2)^{-1}$ increases). This reflects the fact that the gradient growth is stronger in very hyperbolic regions (low $|r|$). More precisely, the gradient not only grows in hyperbolic regions as predicted by the analysis based on $|r|$ but also in elliptic regions, although less strongly. The cascade efficiency continuously increases from zero in strongly elliptic regions ($|r| \gg 1$, $\alpha \approx 0$) then approximately saturates in hyperbolic regions ($|r| < 1$, $\alpha > 1/2$). This is consistent with the analysis of Klein *et al.* (2000) according to which the strain-rate fluctuation expressed by s (equation (2.6)) affects the gradient orientation and growth and must be taken into account in elliptic regions. This effect is not negligible since the cascade efficiency $h(r)$ has already reached roughly 50% of its maximum when $r = 1$ ($\alpha = 1/2$) whereas neglecting the strain-rate fluctuation s as in Lapeyre *et al.* (1999) would lead to $h(r) = 0$ for $|r| > 1$.

The s-conditioned growth rate $h(s)$ is also positive and is found to increase when $|s|$ decreases ($\beta \equiv (1+s^2)^{-1}$ increases). Thus the cascade in elliptic regions is most efficient where the strain rate is most persistent (least fluctuating) in time. However, neither of these two quantities seems to make a significant difference between vorticity (solid) and passive scalar (dashed) in all three experiments. The curves $h_\omega(r)$ and $h_T(r)$ slightly differ in the hyperbolic regions of experiments SMALL and FORCED but not in experiment LARGE. Concerning $h_\omega(s)$ and $h_T(s)$, the differences observed in the three experiments are again not significantly larger than their own fluctuations.

Although our main interest is in the common features of the three experiments, it is instructive to compare the behaviours of $h(r)$ and $h(s)$ in the three regimes. The behaviour of $h(s)$ does not show any qualitative difference between LARGE, SMALL and

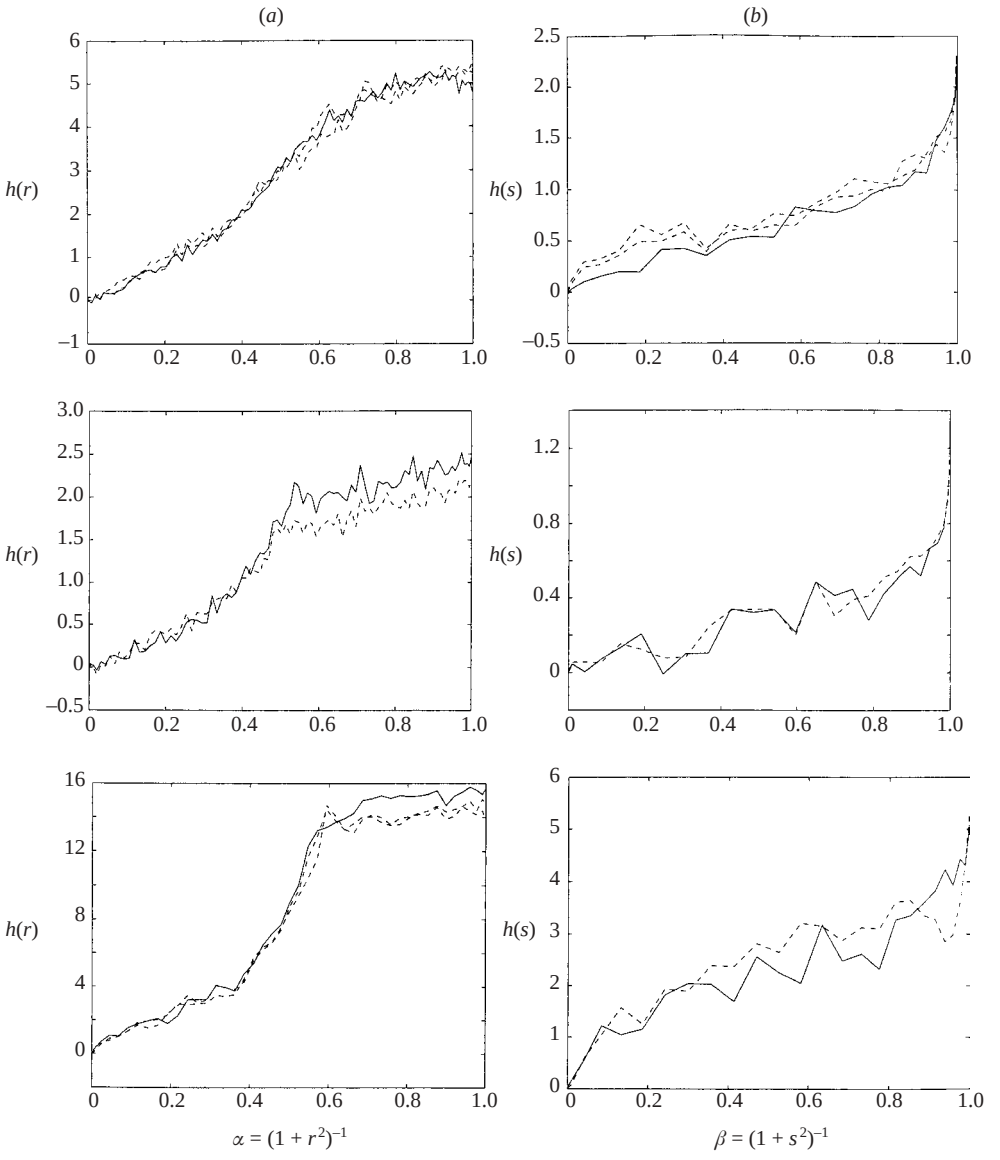

FIGURE 4. Diagnostics $h(r)$ and $h(s)$ (see table 1) based on the first Lagrangian derivative of the squared scalar gradient of vorticity (solid) and passive scalar (dashed). (*a*) Conditional averages with respect to the reduced effective rotation r. The abscissa is $\alpha \equiv (1+r^2)^{-1}$ for graphical convenience. Elliptic regions correspond to $\alpha < 1/2$. (*b*) Conditional averages with respect to the reduced strain-rate fluctuation s and restricted to elliptic regions. The abscissa is $\beta \equiv (1+s^2)^{-1}$. From top to bottom: simulations LARGE, SMALL (both decaying) and FORCED (forced).

FORCED, in contrast to the cascade efficiency h as a function of r. As noticed before, h continuously increases with α. The maximum growth occurs in the weakly elliptic or weakly hyperbolic region $0.4 \leqslant \alpha \leqslant 0.6$. We can observe that this recurrent maximum growth rate is relatively stronger in the FORCED case. This feature is essentially the same for vorticity and passive scalars.

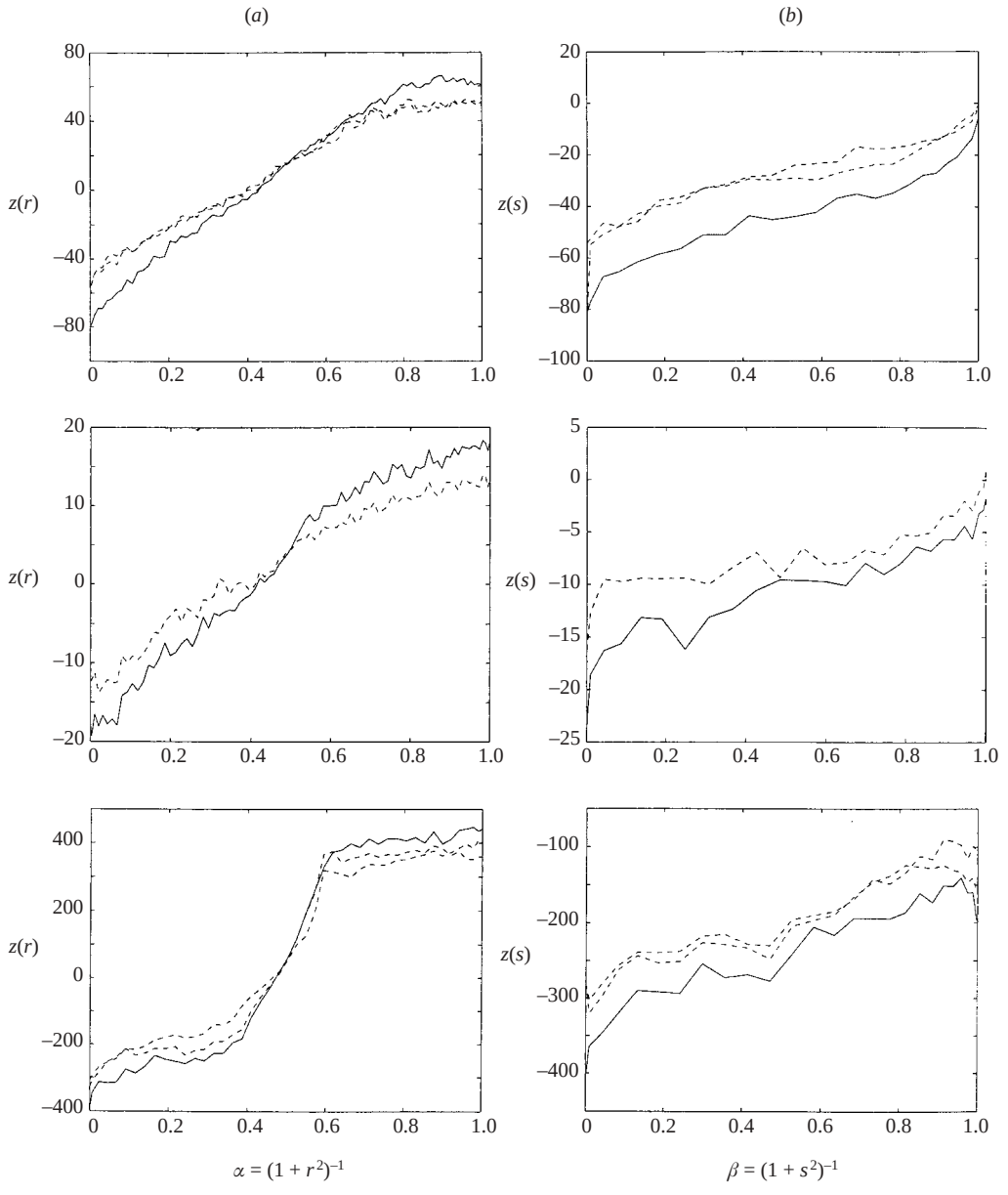

FIGURE 5. Diagnostics $z(r)$ and $z(s)$ (see table 1) based on the second Lagrangian derivative of the squared scalar gradient of vorticity (solid) and passive scalar (dashed). (*a*) Conditional averages with respect to the reduced effective rotation r. The abscissa is $\alpha \equiv (1+r^2)^{-1}$ for graphical convenience. Elliptic regions correspond to $\alpha < 1/2$. (*b*) Conditional averages with respect to the reduced strain-rate fluctuation s and restricted to elliptic regions. The abscissa is $\beta \equiv (1+s^2)^{-1}$. From top to bottom: simulations LARGE, SMALL (both decaying) and FORCED (forced).

4.2.3. *Second-order diagnostics: local cascade fluctuations*

We present in figure 5 the diagnostics based on the second Lagrangian derivative, $z(r)$ (figure 5*a*) and $z(s)$ (figure 5*b*). Experiments LARGE, SMALL and FORCED are presented, from top to bottom. Concerning the r-conditioned growth rate $z(r)$ (column *a*),

one can see as discussed in § 3.1 that it is positive in hyperbolic regions ($\alpha > 1/2$, $|r| > 1$) corresponding qualitatively to an exponential growth of the gradient norm, and negative in elliptic regions, corresponding to a temporal oscillation with a much slower net growth. As a consequence the s-conditioned growth rate $z(s)$, being limited to elliptic regions, is negative too (column *b*).

The qualitative argument developed in § 3.2 suggests that, in elliptic regions, z_T for the passive scalar should be larger (less negative) than z_ω for vorticity. This is indeed what we observe for both diagnostics $z(r)$ and $z(s)$. Concerning $z(r)$, the inequality $z_T(r) > z_\omega(r)$ is satisfied in elliptic domains ($|r| > 1$, $\alpha < 1/2$) and compensated in hyperbolic domains by the converse inequality as is required by the observed equality of the global diagnostics $z_T = z_\omega$.

This inequality is best satisfied for $z(s)$: the conditional averages are performed in elliptic domains only and the inequality $z_T(s) > z_\omega(s)$ is robustly observed in all three simulations. The difference $z_T(s) - z_\omega(s)$ is much higher than the typical fluctuation indicated by the superimposed curves for two different passive scalars (dashed, experiments LARGE and FORCED) and can be higher than 20% of the value of $z(s)$ itself. Interpreting $z(s)$ as giving a time scale for the fluctuations of the gradient, the fact that $z_\omega(s)$ is more negative than $z_T(s)$ indicates that the vorticity gradient has faster temporal fluctuations than the passive scalar gradient.

For completeness, let us mention that the same study performed on random fields does not provide additional information. The curves $z_T(r)$ and $z_\omega(r)$ (not shown) essentially behave as $z_T(\sigma)$ and $z_\omega(\sigma)$ apart from the fact that they are no longer linear. The main property missing in these random flows is that the growth rate for the passive scalar $z_T(r)$ is bound to be positive even in elliptic regions, at contrast to turbulent fields.

Finally, one can examine the sensitivity of the second-order diagnostics to the turbulent regime. Concerning $z(r)$, the main observation is that the r-conditioned growth rate $z(r)$ depends smoothly on r in decaying turbulence (LARGE and SMALL) whereas in the forced case only small variations of $z(r)$ occur inside the elliptic and hyperbolic regimes, which are separated by a sharp transition when $0.4 \leqslant \alpha \leqslant 0.6$.

5. Discussion

We have compared the direct cascades of vorticity and a passive scalar analysed in terms of the growth process of their gradients. This lead us to define diagnostic quantities following two guidelines. First, they make a compromise between the local and global points of view, hence the conditional averages. Second, they only rely on objective (frame-invariant) quantities: Lagrangian time derivatives of the gradient-squared-norm, non-dimensional objective parameters r and s. In a very simple situation, we argued that the second Lagrangian derivative may provide interesting information on the problem at hand, the comparison of the two cascades.

We performed numerical simulations of both forced and free two-dimensional turbulence with different kinds of initial conditions. We diagnosed them, and found that the dynamical nature of vorticity does not consistently appear in a first-order analysis of the Lagrangian dynamics of scalar gradients but is revealed at the second order. Furthermore, the observed passive–active difference is consistent with that previously obtained in a simple situation and indicates that the vorticity gradient has faster temporal fluctuations than the passive scalar gradient.

For smooth velocity fields like those produced by the two-dimensional direct enstrophy cascade, there is an analogy between the relative dispersion of pairs of

particles and the growth of scalar gradients. For certain ranges of scales, the relative dispersion has been observed to be exponential in time (Morel & Larchevêque 1974; Babiano *et al.* 1990). With this in mind, the first-order diagnostic $h(r)$ can be interpreted as an inverse time scale for the exponential growth of the scalar gradient, which is expected to hold in hyperbolic regions (Lapeyre *et al.* 1999). The first-order analysis of the two cascades (figure 4) exhibits differences between vorticity and a passive tracer but not in all of the three numerical experiments. Indeed, one observes that in the hyperbolic domains of experiments SMALL and FORCED the time scale $h^{-1}(r)$ is slightly shorter for vorticity than for the passive scalar. Thus there are signs of an r-dependent exponential behaviour that is slightly different for vorticity and passive scalar gradients, although not in all the cases considered in this work.

Finally, we briefly considered the influence of the turbulent regime on our cascade diagnostics, in addition to our main goal of characterizing the passive–active difference independently of this regime. The turbulent regime unquestionably effects on the scalar cascades and we pointed out two typically different behaviours of $h(r)$ and $z(r)$ in decaying and forced cases. This has a larger impact than the active–passive difference itself, and so the discussion of their dependence on the turbulent regime would be very hazardous without additional specific numerical investigations.

Although we consistently show a difference between the cascades of vorticity and a passive scalar, this was not easy to demonstrate as illustrated by the collapse to a single curve of several first-order diagnostics. One may then wonder how important this difference can be from theoretical and practical points of view. From the theoretical point of view, it is admitted that calculations treating vorticity essentially as a passive scalar stretched by the velocity field (Kraichnan 1971; Falkovich & Lebedev 1994) produce correct predictions at least for the statistical properties of spectra and structure functions, apart from disputed logarithmic corrections (Lindborg & Alvelius 2000; Jullien *et al.* 2000). What we may infer from the present study is that the 'passive vorticity' assumption is probably a good approximation provided second-order Lagrangian dynamics properties are not involved, i.e. suitable to explore global properties and more questionable when addressing issues involving the partition of physical space and coherent structures. From a more practical point of view, it is common in geophysics to consider that the spatial structure of active scalars like density or temperature merely results from passive advection. Here it is important to remark that vorticity is in some sense the most active scalar one can imagine since it completely determines the velocity field. Active scalars like density or temperature act on the velocity field through the buoyancy force but cannot be deduced from it nor vice versa. One may then expect the signature of such active scalars to be even weaker than that produced by vorticity. It is thus reasonable to consider the assumption of passivity to be appropriate, especially compared to other sources of approximation in a geophysical context.

We wish to thank Dr. Lien Hua for active discussions about this work. The paper also benefited from valuable remarks by anonymous referees. This work was supported by the Ministère de l'Éducation Nationale, de la Recherche et de la Technologie (A.C.I. jeunes chercheurs 0693) and by IDRIS, project 940338.

REFERENCES

Babiano, A. 2001 *Turbulent Mixing in Geophysical Flows*. CIMNE, Barcelona.

Babiano, A., Basdevant, C., Legras, B. & Sadourny, R. 1987 Vorticity and passive scalar dynamics in two-dimensional turbulence. *J. Fluid Mech.* **183**, 379–397.

Babiano, A., Basdevant, C., Leroy, P. & Sadourny, R. 1990 Relative dispersion in two-dimensional turbulence. *J. Fluid Mech.* **214**, 535–557.

Basdevant, C. & Philipovitch, T. 1994 On the validity of the "Weiss criterion" in two-dimensional turbulence. *Physica* D **73**, 17–30.

Batchelor, G. K. 1967 *An Introduction to Fluid Dynamics*. Cambridge University Press.

Dresselhaus, E. & Tabor, M. 1991 The stretching and alignment of materiel elements in general flow fields. *J. Fluid Mech.* **236**, 415–444.

Dubos, T. & Babiano, A. 2002 Cascades in two-dimensional mixing: a physical space approach. *J. Fluid Mech.* **467**, 81–100.

Elhmaidi, D., Provenzale, A. & Babiano, A. 1993 Elementary topology of two-dimensional turbulence from a lagrangian viewpoint and single-particle dispersion. *J. Fluid Mech.* **257**, 533–558.

Falkovich, G. & Lebedev, V. 1994 Nonlocal vorticity cascade in two dimensions. *Phys. Rev.* E **49** (3), R1800–1803.

Holloway, G. & Kristmannsson, S. 1984 Stirring and transport of tracer fields by geostrophic turbulence. *J. Fluid Mech.* **141**, 27–50.

Jullien, M.-C., Castiglione, P. & Tabeling, P. 2000 Experimental observation of Batchelor dispersion. *Phys. Rev. Lett.* **85**, 3636–3639.

Klein, P., Hua, B. L. & Lapeyre, G. 2000 Alignment of tracer gradients in two-dimensional turbulence using second order lagrangian dynamics. *Physica* D **146**, 246–260.

Kraichnan, R. 1971 Inertial-range transfer in two- and three-dimensional turbulence. *J. Fluid Mech.* **47**, 525–535.

Lamb, H. 1932 *Hydrodynamics*. Cambridge University Press.

Lapeyre, G., Hua, B. L. & Klein, P. 2001 Dynamics of the orientation of gradients of passive and active scalars in two-dimensional turbulence. *Phys. Fluids* **13**, 251–264.

Lapeyre, G., Klein, P. & Hua, B. L. 1999 Does the tracer gradient align with the strain eigenvectors in 2D turbulence? *Phys. Fluids* **11**, 3729–3737.

Larchevêque, M. 1993 Pressure field, vorticity field and coherent structures in two-dimensional incompressible turbulent flows. *Theor. Comput. Fluid Dyn.* **5**, 215–222.

Lindborg, E. & Alvelius, K. 2000 The kinetic energy spectrum of the two-dimensional enstrophy turbulence cascade. *Phys. Fluids* **12**, 945–947.

Morel, P. & Larchevêque, M. 1974 Relative dispersion of constant-level balloons in the 200 mb general circulation. *J. Atmos. Sci.* **31**, 2189–2196.

Ohkitani, K. 1991 Wave-number space dynamics of enstrophy cascade in a forced two-dimensional turbulence. *Phys. Fluids* A **3**, 1598–1611.

Okubo, A. 1970 Horizontal dispersion of floatable particles in the vicinity of velocity singularities such as convergences. *Deep-Sea Res.* **17**, 445–454.

Protas, B., Babiano, A. & Kevlahan, N. K.-R. 1999 On geometrical alignment properties of two-dimensional forced turbulence. *Physica* D **128**, 169–179.

Provenzale, A. 1999 Transport by coherent barotropic vortices. *Annu. Rev. Fluid Mech.* **31**, 55–93.

Saffman, P. 1971 Spectrum and decay of random two-dimensional vorticity distributions at large Reynolds number. *Stud. Appl. Math.* **50**, 377.

Weiss, J. 1991 The dynamics of enstrophy transfer in two-dimensional turbulence. *Physica* D **48**, 273–294.